Phase transition in ferroelectric Pb(Zr0.52Ti0.48)O3 epitaxial thin films

Qiang Liu, O. Marconot, M. Piquemal, C. Eypert, Alexis Borowiak, Nicolas Baboux, B. Gautier, A. Benamrouche, Pédro Rojo Romeo, Yves Robach, et al.

Phase transition in ferroelectric $Pb(Zr_{0.52}Ti_{0.48})O_3$ epitaxial thin films

Q. Liu [a], O. Marconot [a], M. Piquemal [a], C. Eypert [b], A.S. Borowiak [c], N. Baboux [c], B. Gautier [c], A. Benamrouche [a], P. Rojo-Romeo [a], Y. Robach [a], J. Penuelas [a], B. Vilquin [a,*]

[a] Université de Lyon, Ecole Centrale de Lyon, Institut des Nanotechnologies de Lyon, CNRS UMR 5270, 69134 Ecully cedex, France
[b] Horiba Scientific, Avenue de la Vauve, Passage Jobin Yvon, 91120, Palaiseau, France
[c] Université de Lyon, INSA de Lyon, Institut des Nanotechnologies de Lyon, CNRS UMR 5270, 69621 Villeurbanne, France

$PbZr_{1-x}Ti_xO3$ (PZT) has been intensively studied for various ferroelectric applications. Its promising application for micro-electro-mechanical system has reignited the interests due to its outstanding ferroelectric and piezo-electric properties. Most PZT ceramics employed in devices are synthesized with a Zr/Ti ratio close to the tetrag-onal–rhombohedral morphotropic phase boundary ($x = 0.48$) due to its high electro-mechanical coupling at this composition. Morphotropic phase boundary is particularly interesting to study for the investigation of phase transition. In this work, we report the epitaxial growth and electrical characterization of epitaxial PZT (Zr/Ti = 52/48) thin films on Nb-doped SrTiO3. PZT films, with thickness from 30 nm to 65 nm, were deposited by sol–gel method and eventually crystallized at 700 °C by rapid thermal annealing in oxygen. Film ferroelectric-ity was confirmed by Sawyer–Tower circuit measurement. X-ray diffraction analysis indicates a thickness-dependent structural phase, i.e., a phase transition from tetragonal phase for the thinner film to a biphasic (tetragonal + pseudo-cubic) structure for the thicker film, which is characterized by ellipsometry as a phase separation from the bottom surface of the film to the top one. This phase transition is related to a composition gradient within the film thickness.

1. Introduction

Lead zirconate titanate ($PbZr_{1-x}Ti_xO_3$ or PZT) ferroelectric thin films have been extensively studied in the past thirty years due to their potential applications, such as ultrasonic transducer [1], accelerometer [2,3], micro pump [4], gas sensors [5], electro-optic modulator [6] and energy harvesting [7]. For most of their applications, the use of bulk materials has already existed for a long period. Miniaturization of such devices into micro-electromechanical systems by using thin films will benefit from the requirement of exchanging minimal amount of energy and obtaining improved performances, like high resonance frequencies, low operation voltages, and high sensitivities [8,9]. One of the commonly studied chemical compositions is $PbZr_{0.52}Ti_{0.48}O_3$ because of the presence of the morphotropic phase boundary (MPB) between the Zr-rich rhombohedral phase and the Ti-rich tetragonal phase. Near MPB, PZT material exhibits an average crystalline structure, which can be characterized by macroscopic measurement, like conventional X-ray diffraction (XRD), involving both tetragonal and rhombohedral lattices. Both PZT phases are energetically favourable in this case, so there are totally 14 possible orientations of spontaneous polarization and, thus, the piezoelectric and ferroelectric performance are largely enhanced [10]. In addition, high-resolution synchrotron XRD reveals a local monoclinic crystalline structure in PZT material near MPB [11]. In Zr-rich composition, local monoclinic lattices distributed randomly with three preferred orientations result in the rhombohedral symmetry [12], while in Ti-rich composition local monoclinic lattices with four preferred orientations result in the tetragonal symmetry [13]. Such monoclinic phase exists within a certain width in the chemical composition near MPB, which generally becomes narrow with increasing the temperature.

In this work, epitaxial single crystal PZT thin films with the MPB chemical composition were grown on Nb doped $SrTiO_3$ (Nb-STO) substrate by sol–gel method. Electric field induced polarization (P–E loop) displayed a typical ferroelectric hysteresis loop and low leakage current was observed for these PZT films. As the thickness increases, we found a phase transition from tetragonal phase for the thinner film to a biphasic (tetragonal + pseudo-cubic) structure for the thicker film, which is related to a thickness-dependent phase separation involved by a Zr/Ti composition gradient. Furthermore, ferroelectric domain was created by applying a dc voltage via a piezoresponse force microscopy (PFM) setup, by which the local ferroelectric properties are studied.

2. Experimental details

Sol–gel method combined with spin-coating was employed in this study to fabricate PZT thin films on conductive Nb-STO substrate. The precursor solution from *Mitsubishi Chemical Inc.* consists of several organometallic compounds, i.e., lead acetate ($Pb(CH_3COO)_2$), zirconium tetra-n-butoxide ($Zr(OC_4H_9)_4$), and titanium tetra-iso-propoxide

* Corresponding author.
E-mail address: bertrand.vilquin@ec-lyon.fr (B. Vilquin).

$(Ti(OCH(CH_3)_2)_4)$, as starting materials which are dissolved in isopropanol alcohol ($(CH_3)_2CHOH$). This precursor solution was designed at Queen's University in 1988 [14]. It has the property of acetic acid to slow the hydrolysis and the condensation reactions of transition metal alkoxides by forming more stable metal alkoxo-acetylates [15]. Chemical composition of the solution is consistent with the stoichiometry of the final PZT film except that 10% extra Pb is intentionally added to redeem the loss during thermal treatment, namely Pb:Zr:Ti = 110:52:48 for PZT film at MPB. After spin coating, calcination at 300 °C during 5 min in air was carried out, followed by an annealing at 700 °C during 1 min with oxygen in a rapid thermal annealing (RTA) furnace. The film thickness of three as-deposited PZT samples measured by X-ray reflectivity is respectively 30 nm, 45 nm, and 65 nm, corresponding to the spin-coating rotation speed at 6000 rpm, 3000 rpm, and 1500 rpm.

Surface morphology after PZT deposition was obtained by Veeco CP II AFM (atomic force microscopy) in non-contact mode. Crystalline structure of these PZT thin films was investigated using a Rigaku SmartLab high-resolution diffraction system with *Cu* $K_{\alpha 1}$ radiation via $2\theta/\omega$ scan and reciprocal space mapping. For electrical characterization, 250 nm-thick Pt top electrode with an area of $100 \times 100\ \mu m^2$ was fabricated by lift-off process on PZT surface. Electrical properties in macroscopic scale were studied by using Sawyer–Tower method to obtain the electric field induced polarization (P–E loop) at room temperature with a NF-WF-1966 2-chanel generator and a Nicolet INTEGRA-40 oscilloscope. Finally optical characterization was carried out by spectroscopic ellipsometry to examine the thickness-dependent phase transition, where a phase modulated spectroscopic ellipsometer from Horiba Scientific, UVISEL ER was used.

3. Results and discussion

3.1. XRD characterization

Fig. 1 shows the out-of-plane XRD $2\theta/\omega$ scan on these as-grown PZT thin films. We see that only one Bragg peak of PZT (002) appears for the 30 nm-PZT sample, corresponding to the single-domain tetragonal phase. From the thickness of 45 nm, a separation of PZT (002) Bragg peak is observed, indicating a second PZT phase within the film. Moreover, the separation of PZT (002) Bragg peak is more evident for the 65 nm one. The out-of-plane lattice parameter is 0.411 nm in the tetragonal PZT phase, and is 0.407 nm in the second PZT phase for both 45 nm-PZT and 65 nm-PZT. In the in-plane XRD measurement (not shown), only one lattice parameter is found for all the three samples, indicating that the second PZT phase has the same in-plane lattice parameter as the tetragonal PZT phase, i.e. 0.407 nm. As the second PZT phase has the equal value for in-plane and out-of-plane lattice parameters, this phase is supposed to have a pseudo-cubic perovskite structure, i.e. corresponding to the PZT rhombohedral phase [16].

Texture structure of these three PZT samples was further characterized by reciprocal space mapping (RSM) around PZT (103) Bragg spots, which are shown in Fig. 2. For the thinnest film, the PZT (103) Bragg spots with an ellipse-like shape suggest a homogeneous epitaxial PZT crystalline structure near the tetragonal-domain PZT structure. For the 45 nm-thick and 65 nm-thick films, the PZT (103) Bragg spots are deformed with the appearance of a second Bragg spot, corresponding to a pseudo-cubic perovskite phase [16]. These results are in agreement with the $2\theta/\omega$ scan XRD where the PZT film structure evolves from a single phase (tetragonal phase) to a bi-phase (tetragonal + pseudo-cubic). From the RSM measurements, one can see that all the PZT films are relaxed on Nb-STO substrate. This phenomenon is similar to the PZT (20/80) thin films reported in Ref. [17,18] where all the thicknesses are below 50 nm, show strain relaxation process that the thickest films are almost strain relaxed.

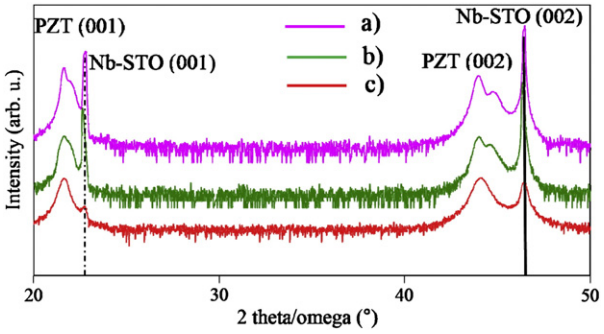

Fig. 1. $2\theta/\omega$ XRD patterns of (a) 30 nm-PZT; (b) 45 nm-PZT; (c) 65 nm-PZT.

3.2. AFM characterization

Surface morphology of the as-grown PZT thin films was characterized by the AFM setup (not shown). We found that the grain size increased as the thickness increased from 30 nm to 65 nm. The RMS (root mean square) values of the surface roughness are 0.77 nm for the 30 nm-PZT, 0.92 nm for the 45 nm-PZT, and 1.20 nm for the 65 nm-PZT, respectively. It increases slightly as the thickness increases, but the surface roughness agrees well with the previous results published for similar PZT composition and film thickness [19].

3.3. Ferroelectric characterization

Ferroelectric hysteresis loops were obtained using Sawyer–Tower method [20] on 45 nm-PZT sample which was deposited Pt top electrode using sputtering. Fig. 3 shows the P–E loop measured under different ranges of the applied voltage from 2 V to 6 V. Anti-clockwise hysteresis loops are observed, which are induced by the PZT ferroelectric domain switching. The induced polarization increases as the voltage augments and, moreover, the hysteresis loop is almost saturated when the voltage rises up to 6 V (1333 kV/cm), i.e. a maximum polarization of 45 $\mu C/cm^2$. The saturated polarization value agrees well with the previous results reported in Ref. [21] where the PZT films with the same Zr/Ti chemical composition were fabricated. PFM measurement performed on the same PZT sample (not shown) exhibits a homogeneous piezoelectric response on the surface. As the rhombohedral and tetragonal phases do not possess the same remnant polarization and the orientation, one can suppose that only one of the two PZT phases is present near the sample surface.

3.4. Spectroscopic ellipsometry characterization

Spectroscopic ellipsometry (SE) is a non-destructive technique and measures the change in the polarization state of light that is reflected from a sample. The change of polarization is described by the amplitude ratio, $\tan\Psi = |r_p|/|r_s|$, of the resolved components of the electric vector parallel to and perpendicular to the plane of incidence, and the phase difference, $\Delta = \delta_p - \delta_s$, between both components. The ellipsometric data is usually expressed in the ρ-representation:

$$\rho = r_p/r_s = \left(|r_p|e^{i\delta_p}\right)/\left(|r_s|e^{i\delta_s}\right) = \tan\Psi e^{i\Delta}, \quad (1)$$

where r_p and r_s represent the complex reflection coefficients for light polarized parallel and perpendicular to the plane of incidence, respectively [22].

I_s and I_c equations are given by: $I_s = \sin 2\Psi \cdot \sin\Delta$ and $I_c = \sin 2\Psi \cdot \cos\Delta$

The measurements were performed over the wide spectral range 0.6 − 6.5 eV (190 nm−2100 nm) with a 1 mm^2 spot size at three incident angles (60°, 65° and 70°) to investigate accurate determination of film properties. SE is sensitive to thickness, optical constants and surface

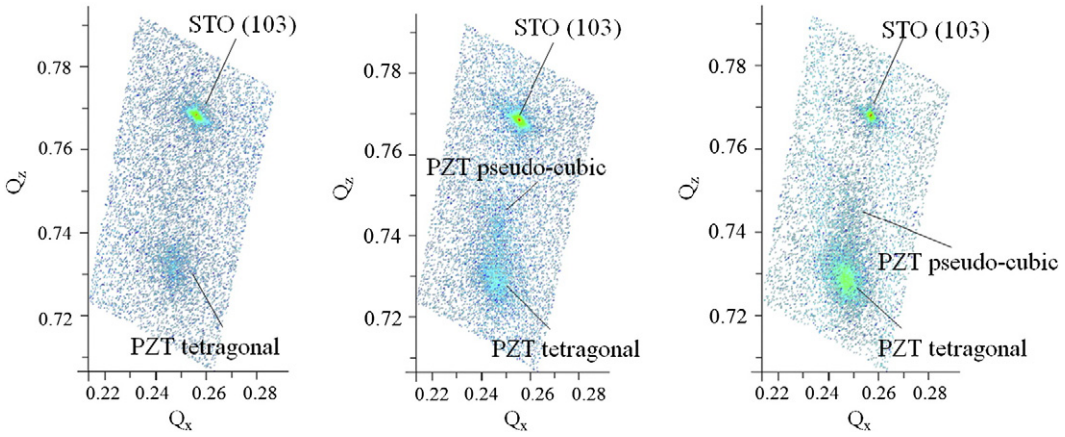

Fig. 2. Reciprocal space maps along STO (103). Intensities from low to high: blue, green, yellow, red. a) 30 nm-PZT; b) 45 nm-PZT; c) 65 nm-PZT.

roughness of thin films. To get these parameters, a model is built and the fit process consists to adjust the experimental data to the generated data. The 30 nm-PZT and 45 nm-PZT samples have been modeled as one homogeneous layer of PZT on $SrTiO_3$ whereas 65 nm-PZT sample has been modeled as one non homogeneous layer, showing a variation of refractive index in the depth. This variation is described by a gradient profile, which reveals a decrease of optical refractive index from the bottom to the surface. Fig. 4 shows the fit results of (Is,Ic) at the three incident angles for 30 nm and 65 nm thick samples. The use of an appropriate dispersion formula has allowed to determine the complex refractive index (n,k) of each PZT samples, as displayed on Fig. 5. These optical constants show a shift of the band gap value to higher energies when the thickness increases. It might explain the coexistence of two phases in PZT film, where each has its own band gap value. Indeed, the PZT optical constants are strongly depending on the Zr/Ti ratio [23]: tetragonal phase has a higher *n* index value than rhombohedral one. As a consequence, the gradient composition should be Ti-rich from bottom to Zr-rich at the surface of the sample.

4. Discussion

Internal stress in the films can induce position shift of the MPB between tetragonal and rhombohedral phases in PZT (52/48), as suggested by Amin et al. [24]. This can be the explanation of the appearance of the second PZT phase in the film. However, as shown by the RSM measurements (Fig. 2), all of our three PZT films are relaxed on the substrate. A better approach can be found in the formation of a chemical composition gradient within the PZT film, ranging from the Ti-rich part, i.e. tetragonal phase, near the substrate to the Zr-rich part, i.e. rhombohedral phase, near the top surface [25]. An attempted explanation is that the formation of the tetragonal phase near the substrate is due to the fact that the activation energy of nucleation is smaller for Ti-rich PZT phase and also the crystallization process is more exothermic than that of Zr-rich PZT phase. This explanation is well confirmed by our spectroscopic ellipsometry, where the bottom part of the PZT film is measured as Ti-rich phase, confirming that a phase transition from tetragonal structure near the Nb-STO/PZT interface to a rhombohedral one near the top surface occurs in the PZT film thicker than 30 nm. This phase transition is a consequence of Zr/Ti composition gradient along the film depth. Besides, one could notice that even for the thickest sample, i.e. 65 nm-PZT, the film remains completely strained on the Nb-STO substrate. This can be attributed to stress relaxation through the

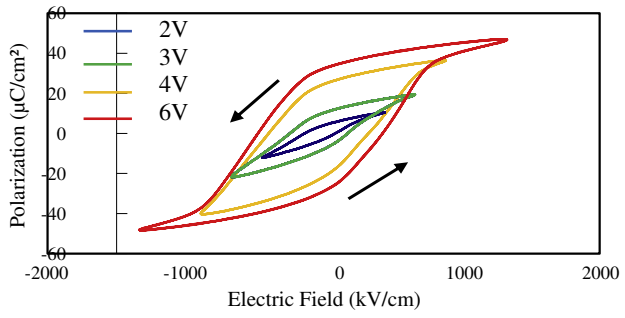

Fig. 3. P–E loops under different voltages (2 V/3 V/4 V/6 V) of Pt/PZT/Nb-STO structure measured at 100 kHZ.

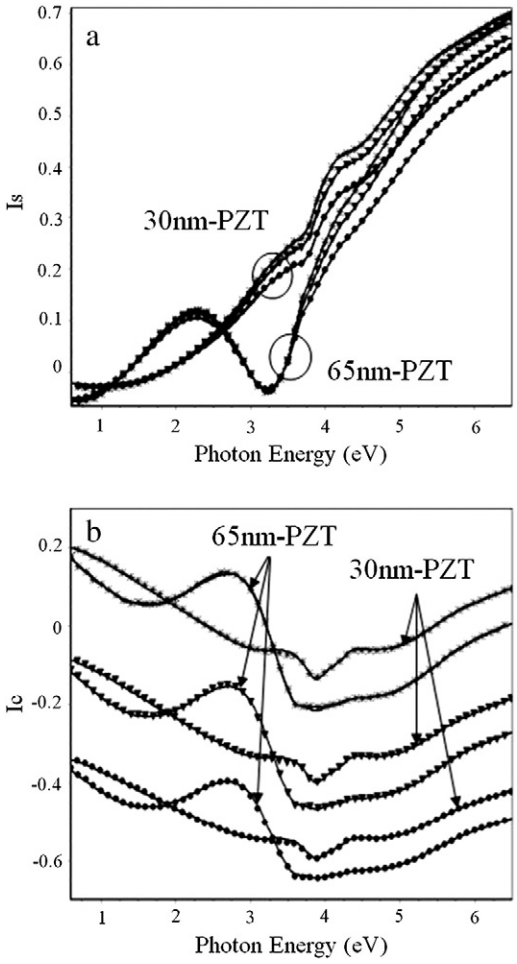

Fig. 4. Ellipsometric fit results for 30 nm and 65 nm PZT. a) Fit results of Is = f(eV); b) Fit results of Ic = f(eV) (Tested at three different incident angles: cross for 60°, solid triangle for 65°, solid circle for 70°.)

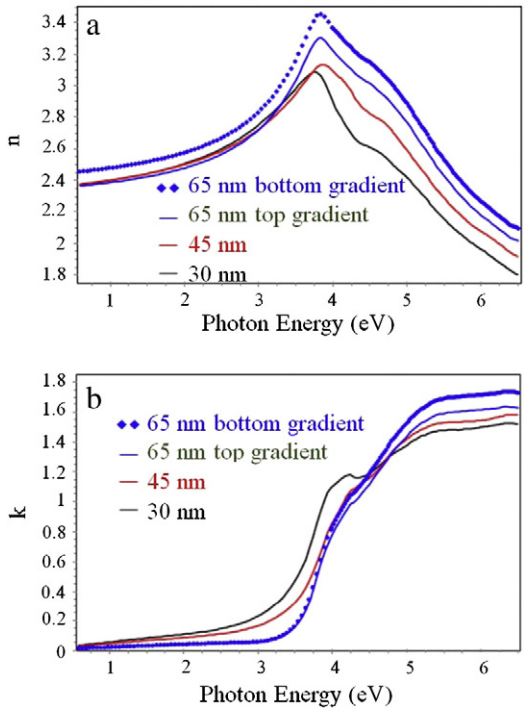

Fig. 5. a) Refractive index *n* of 30 nm, 45 nm and 65 nm-thick PZT; b) Extinction coefficient *k* of 30 nm, 45 nm and 65 nm-thick PZT.

crystallization of the biphasic structure, as it has been already described as the formation of alternative a/c ferroelectric domains in PZT (20/80) films [26].

5. Conclusion

Ferroelectric $Pb(Zr_{0.52}Ti_{0.48})O_3$ thin films were epitaxially grown on Nb-STO substrate using sol–gel method. PZT layers with three different thicknesses, from 30 nm to 65 nm, were crystallized under the RTA treatment at 700 °C for 1 min. Smooth surfaces were obtained with the RMS roughness less than 1.5 nm for all three samples. From XRD characterizations, a second PZT phase with rhombohedral lattice structure was found in 45 nm-PZT and 65 nm-PZT. The existence of a composition gradient from the bottom to the top surface in two thicker PZT samples was confirmed by the optical constants' variation along the depth using spectroscopic ellipsometry.

Acknowledgments

This work, partly realized on NANOLYON platform, was supported by the French Agence Nationale de la Recherche (ANR) through the project PIEZO2POWER, reference: ANR-11-NANO-0015. The authors are very grateful to R. Mazurczyk for his technical help. One of the authors (Q. Liu) would like to thank the Chinese Scholarship Council (CSC) for its financial support.

References

[1] P.A. Payne, J.V. Hatfield, A.D. Armitage, Q.X. Chen, P.J. Hicks, N. Scales, IEEE Ultrason. Symp. 3 (1994) 1523.
[2] L. Wang, R.A. Wolf, Y. Wang, K.K. Deng, L. Zou, R.J. Davis, S. Trolier-McKinstry, J. Microelectromech. Syst. 12 (2003) 433.
[3] H. Yu, L. Zou, K. Deng, R. Wolf, S. Tadigadapa, S. Trolier-McKinstry, Sensors Actuators A Phys. 107 (2003) 26.
[4] K. Uchino, Piezoelectric Actuators and Ultrasonic Motors, Springer, Kluwer, Boston, 1997.
[5] N. Ledermann, P. Muralt, J. Baborowski, M. Forster, J. Pellaux, J. Micromech. Microeng. 14 (2004) 1650.
[6] N. Ledermann, P. Muralt, J. Baborowski, M. Forster, J. Pellaux, J. Micromech. Microeng. 14 (2004) 165.
[7] H. Fang, J. Liu, Z. Xu, L. Dong, L. Wang, D. Chen, B. Cai, Y. Liu, Microelectron. J. 37 (2006) 1280.
[8] M. Li, H.X. Tang, M.L. Roukes, Nat. Nanotechnol. 14 (2007) 114.
[9] S. Trolier-McKinstry, P. Muralt, J. Electroceram. 12 (2004) 7.
[10] A.B.M. Ibrahim, R. Murgan, M.K.A. Rahman, J. Osman, in: M. Lallart (Ed.), Ferroelectric Materials in Ferroelectrics - Physical Effects, InTech Publishing, Croatia, 2011, p. 3.
[11] B. Noheda, D.E. Cox, G. Shirane, R. Guo, B. Jones, L.E. Cross, Phys. Rev. B 63 (2000) 014103.
[12] D.L. Corker, A.M. Glazer, R.W. Whatmore, A. Stallard, F. Fauth, J. Phys. Condens. Matter 10 (1998) 6251.
[13] B. Noheda, J.A. Gonzalo, L.E. Cross, R. Guo, S.-E. Park, D.E. Cox, G. Shirane, Phys. Rev. B 61 (2000) 8687.
[14] G. Yi, Z. Wu, M. Sayer, J. Appl. Phys. 64 (1988) 2717.
[15] J. Livage, M. Henry, C. Sanchez, J. Phys. Solid State Chem. 18 (1988) 299.
[16] G. Leclerc, G. Poullain, R. Bouregba, D. Chateigner, Appl. Surf. Sci. 255 (2009) 4293.
[17] S. Gariglio, N. Stucki, G. Triscone, J.-M. Triscone, Appl. Phys. Lett. 90 (2007) 202905.
[18] H.N. Lee, S.M. Nakhmanson, M.F. Chisholm, H.M. Christen, K.M. Rabe, D. Vanderbilt, Phys. Rev. Lett. 98 (2007) 217602.
[19] K. Aoki, Y. Fukuda, K. Numata, A. Nishimura, Jpn. J. Appl. Phys. 34 (1995) 746.
[20] C.B. Sawyer, C.H. Tower, Phys. Rev. 35 (1930) 269.
[21] C.M. Foster, G.R. Bai, R. Csencsits, J. Vetrone, R. Jammy, L.A. Wills, E. Carr, J. Amano, J. Appl. Phys. 81 (1997) 2349.
[22] A.R. Forouhi, I. Bloomer, Phys. Rev. B34 (1986) 7018.
[23] M.P. Moret, M.A.C. Devillers, K. Worhoff, P.K. Larsen, J. Appl. Phys. 92 (2002) 468.
[24] A. Amin, R.E. Newnham, L.E. Cross, Phys. Rev. B 34 (1986) 1595.
[25] N. Ledermann, P. Muralt, J. Baborowski, S. Gentil, K. Mukati, M. Cantoni, A. Seifert, N. Setter, Sensors Actuators A 105 (2003) 162.
[26] C.M. Foster, W. Pompe, A.C. Daykin, J.S. Speck, J. Appl. Phys. 79 (1996) 1405.